Electronic supporting information

Unravelling mass transport in hierarchically porous catalysts

Mark A. Isaacs,[a] Neil Robinson,[b] Brunella Barbero,[c] Lee J. Durndell,[d] Jinesh Manayil,[c] Chris Parlett,[e.f] Carmine D'Agostino,[e*] Karen Wilson,[g] Adam F. Lee[g*]

[a]*Department of Chemistry, University College London, 20 Gordon Street, Kings Cross, London, WC1H 0AJ, UK*

[b]*Department of Chemical Engineering and Biotechnology, University of Cambridge, Phillipa Fawcett Dr., Cambridge, CB3 0AS, UK*

[c]*European Bioenergy Research Institute, Aston University, Birmingham, B4 7ET, UK*

[d]*dSchool of Geography, Earth and Environmental Sciences, University of Plymouth, Plymouth PL4 8AA, UK*

[e]*School of Chemical Engineering and Analytical Science, University of Manchester, M13 9PL, UK*

[J]*Diamond Light Source Ltd, Harwell Science and Innovation Campus, Didcot OX11 0DE., UK*

[g]*School of Science, RMIT University, Melbourne, VIC3000, Australia*

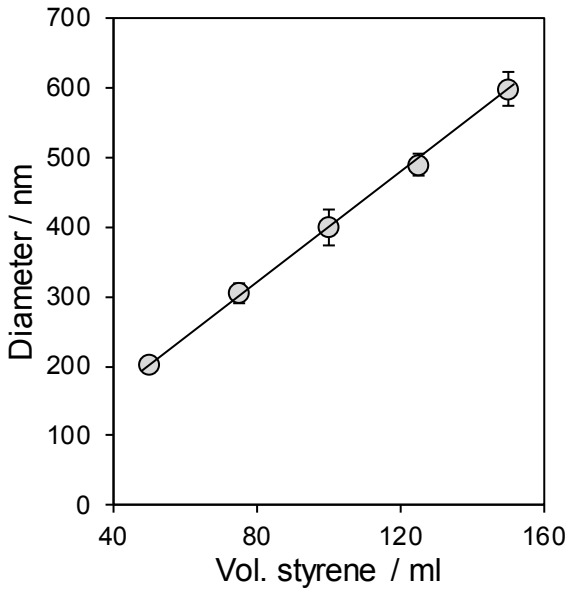

Figure S1. Arithmetic mean polystyrene bead diameter as a function of styrene monomer amount during emulsion polymerisation as determined by TEM.

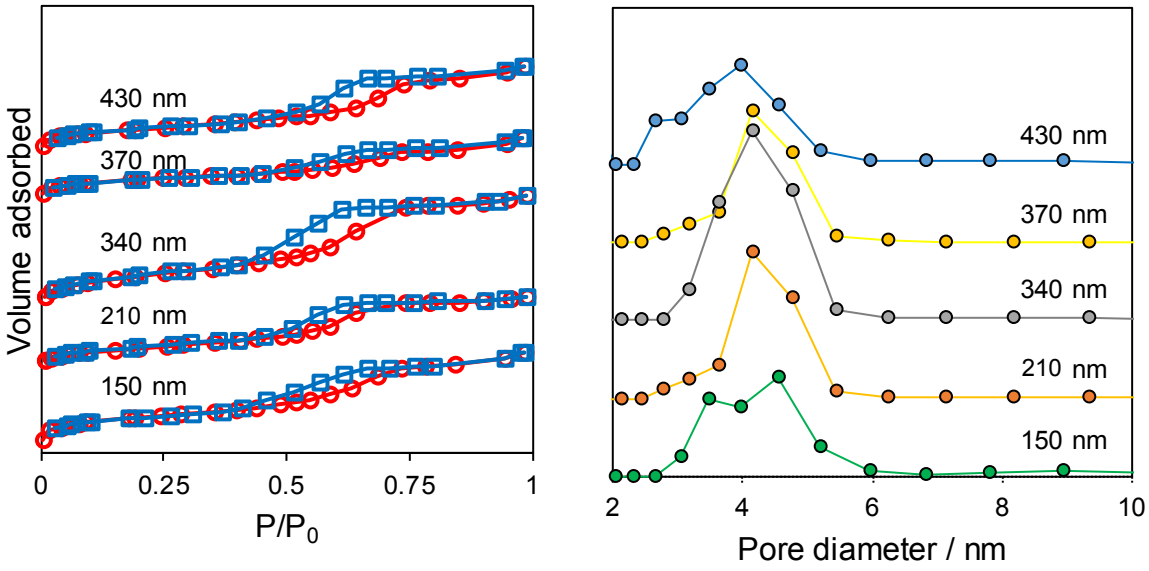

Figure S2. (left) N_2 adsorption-desorption isotherms, and (right) corresponding BJH mesopore size distributions for hierarchically porous MM-SBA-15 as a function of macropore diameter.

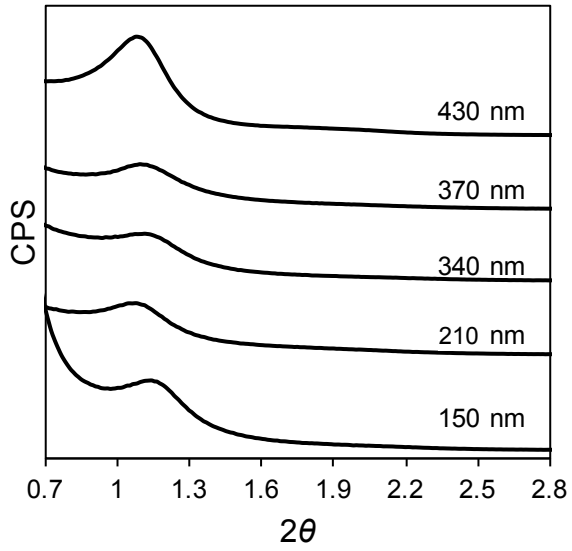

Figure S3. Low angle powder XRD patterns for hierarchically porous MM-SBA-15 as a function of macropore diameter.

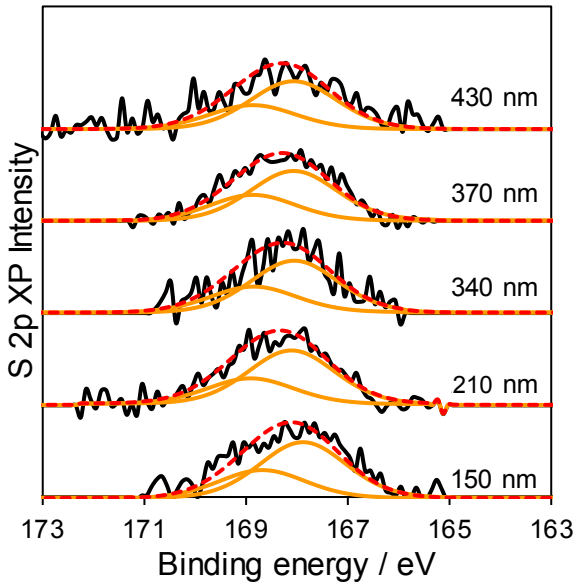

Figure S4. S 2p XP spectra for $PrSO_3H$-MM-SBA-15 as a function of macropore diameter, evidencing only surface sulfonic acid functions.

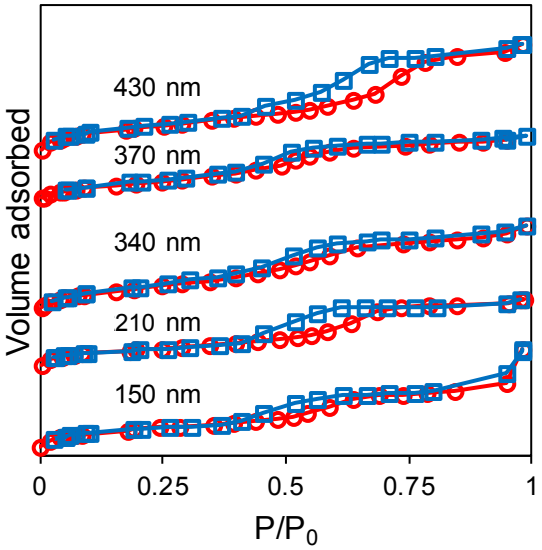

Figure S5. N_2 adsorption-desorption isotherms for $PrSO_3H$-MM-SBA-15 as a function of macropore diameter.

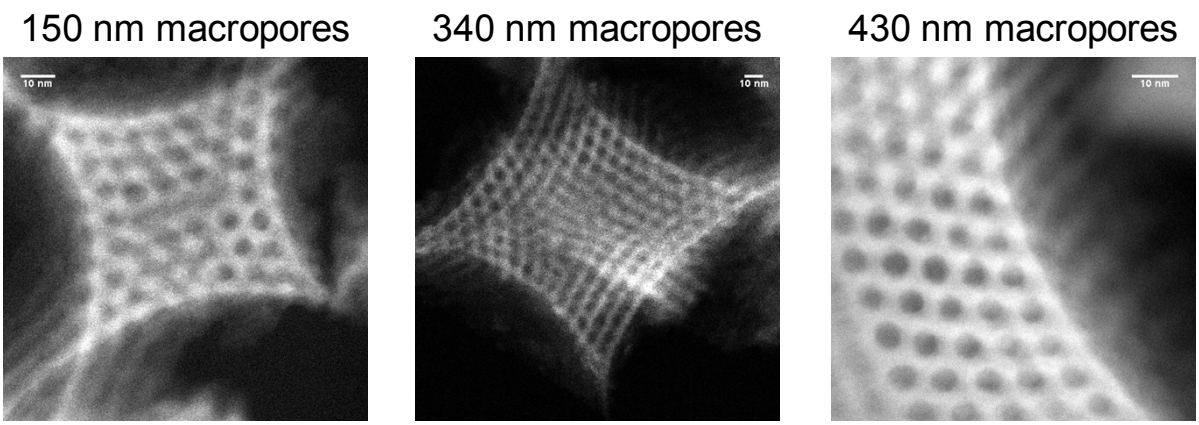

Figure S6. HAADF-STEM images of the macropore-mesopore interface within $PrSO_3H$-MM-SBA-15.

Table S1. Surface areas and bulk and surface sulphur loadings for hierarchically porous MM-SBA-15.

Macropore size / nm	Surface area / $m^2.g^{-1}$ [a]	S wt.% bulk[b]	S wt.% surface[c]	% surface area mesopores[d]	mesopore surface area / $m^2.g^{-1}$
150	215	1.3	0.8	92	198
210	220	1	0.75	94	207
340	260	0.85	0.6	97	252
370	200	0.95	0.7	98	195
430	195	1.25	0.8	98	191

[a]N_2 porosimetry; [b]CHNS; [c]XPS; [d]BJH analysis

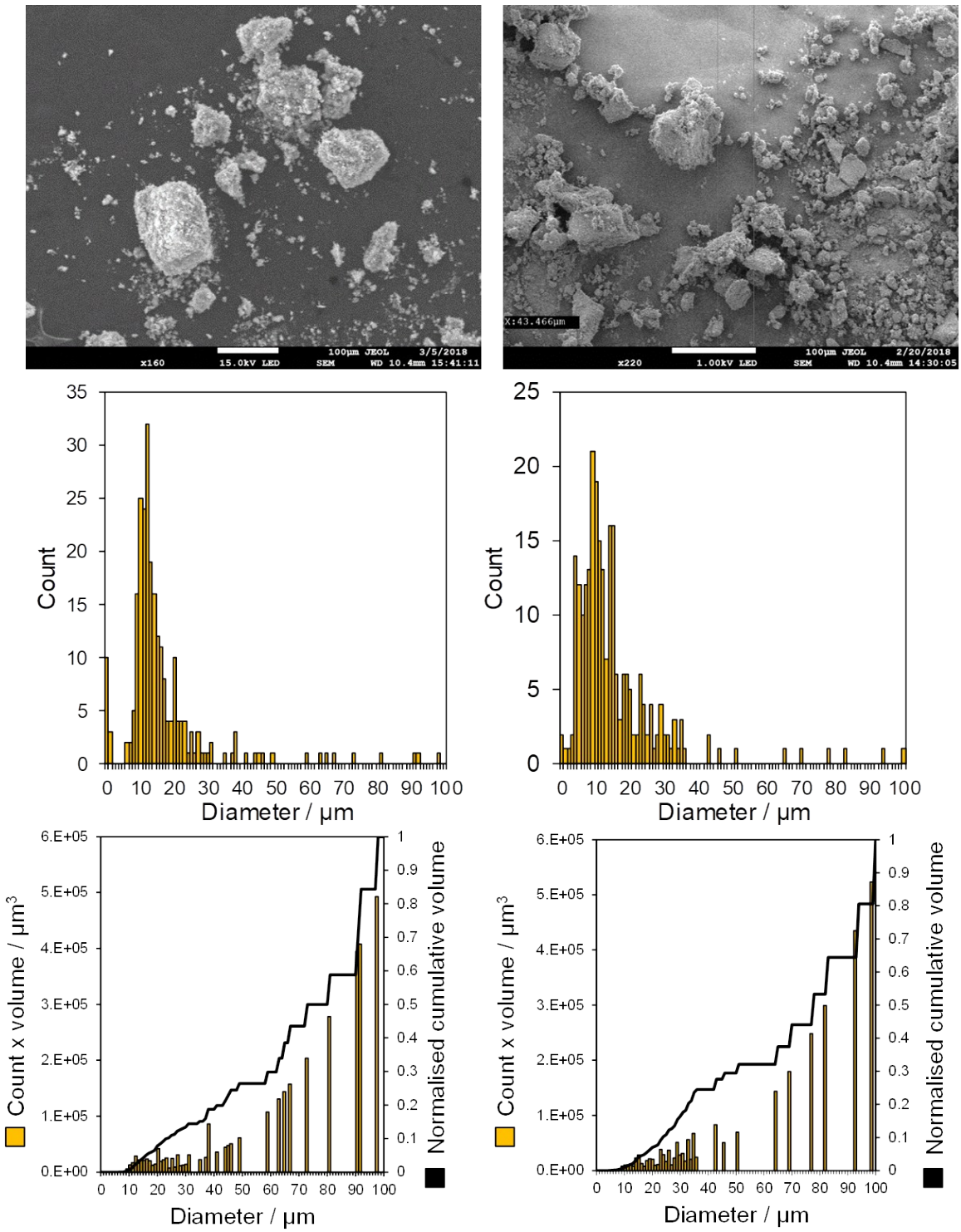

Figure S7. Low magnification SEM images of (top left) 150 nm macropore and (top right) 430 nm macropore MM-SBA-15, and corresponding particle size distributions for (middle left) 150 nm macropore MM-SBA-15 and (middle right) 430 nm macropore MM-SBA-15. Estimated particle volume distributions for (bottom left) 150 nm macropore MM-SBA-15 and (bottom right) 430 nm macropore MM-SBA-15 were calculated assuming spherical particles, and indicate that ≥ 98% of the acquired NMR signal (proportional to available void fraction for liquid-saturated porous media) originates from particles of diameter greater than the modal value of ~12 µm. Histograms were produced from counts of >200 particles.

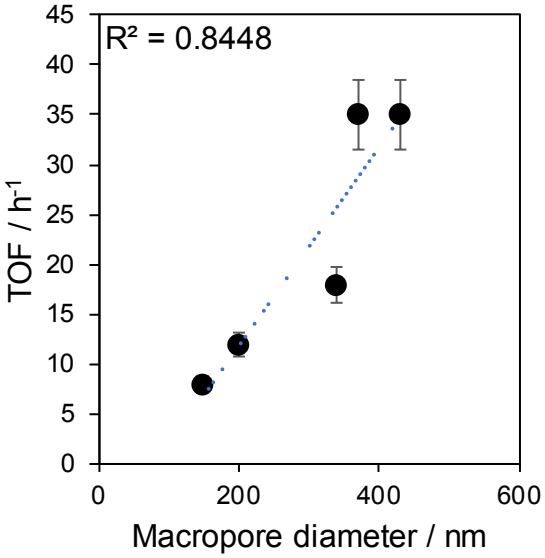

Figure S8. TOF versus macropore diameter for palmitic acid esterification over $PrSO_3H$-MM-SBA-15.

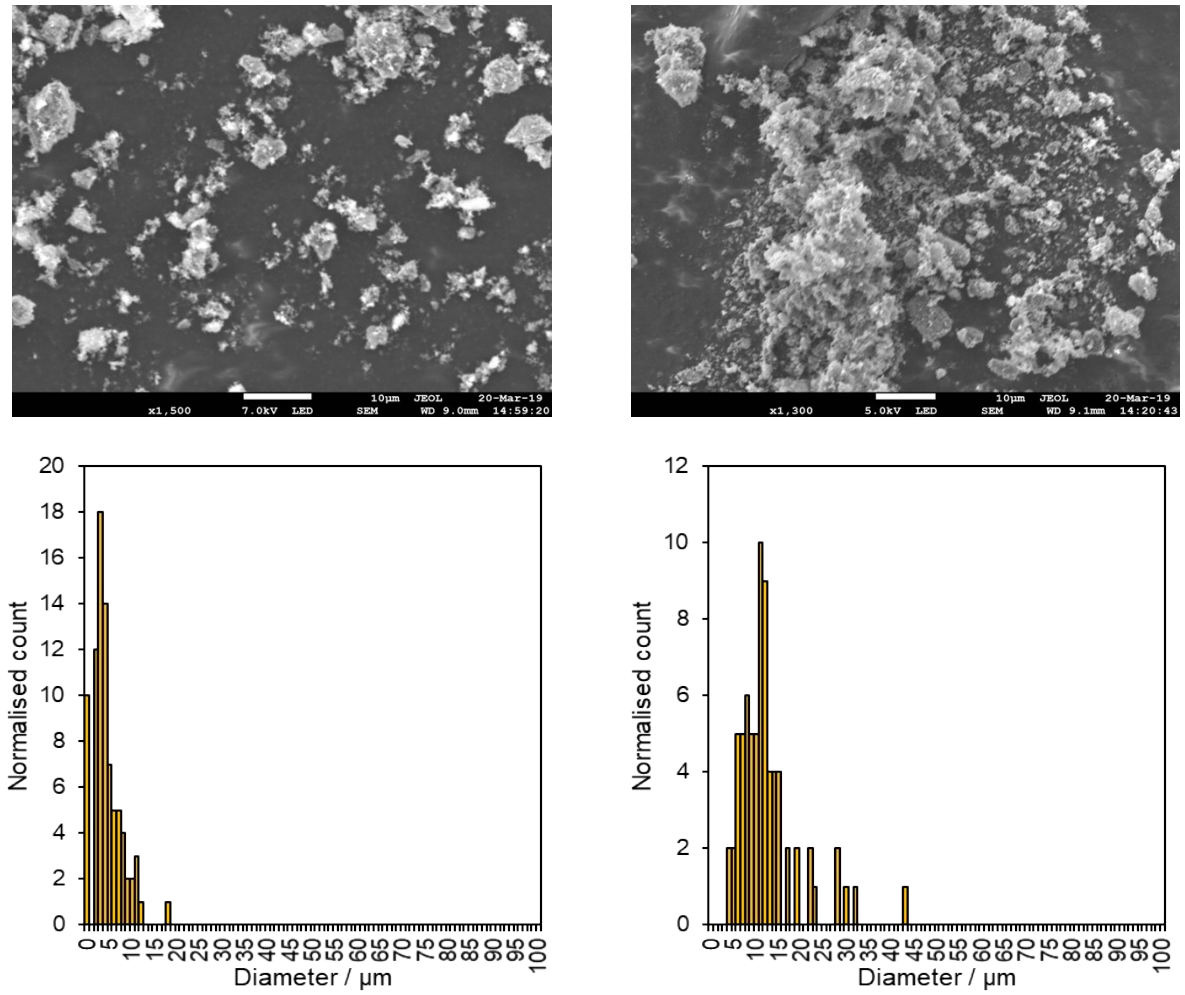

	Average size / µm	StDev / µm
Ground	4.89	3.05
Unground	14.15	15.79

Figure S9. Low magnification SEM images of 210 nm macropore MM-SBA-15 (top left) before and (top right) after mechnical grinding, and corresponding particle size distributions for of 210 nm macropore MM-SBA-15 (bottom left) before and (bottom right) after manual grinding. Histograms were produced from counts of >200 particles.

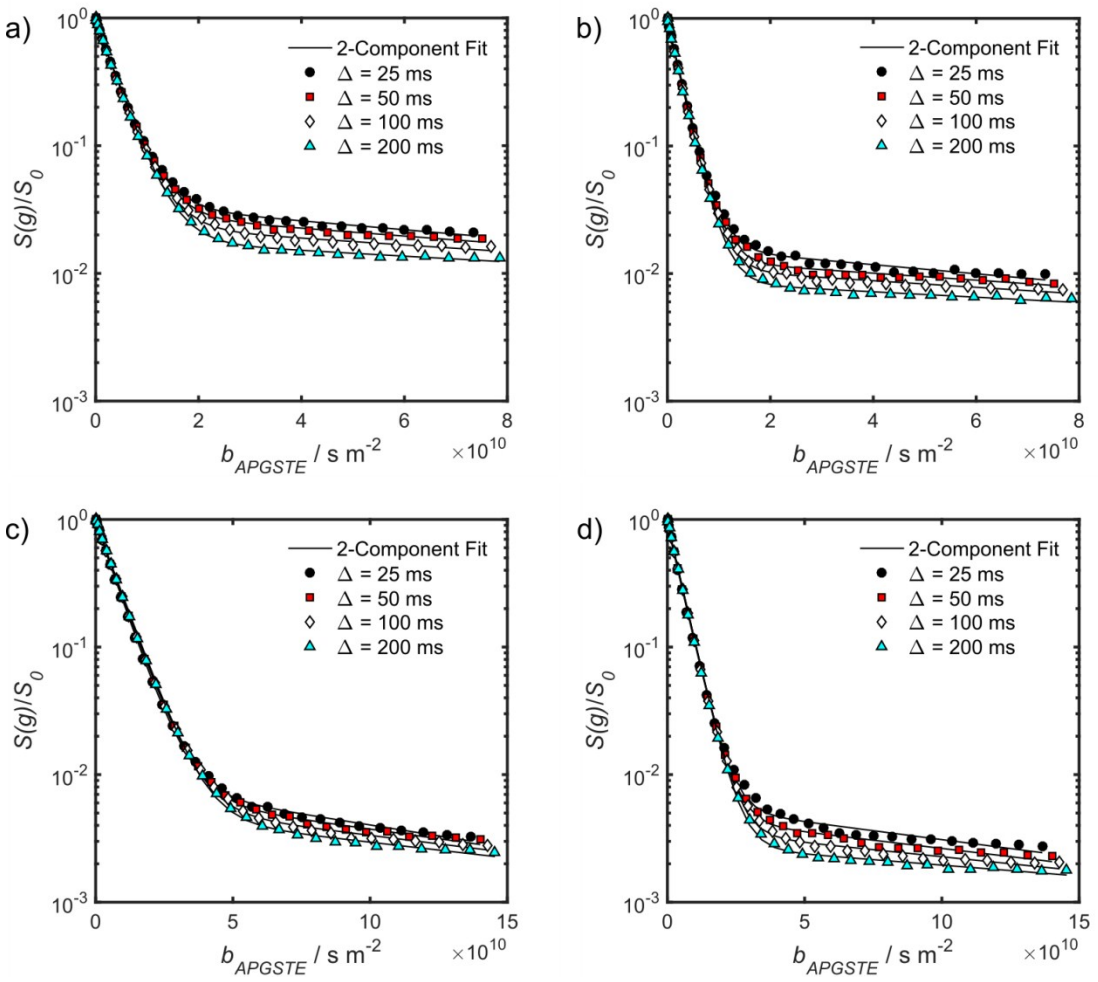

Figure S10. Biexponential fits of the general form $S(g)/S_0 = p_{fast}\exp\{-bD_{fast}\} + p_{slow}\exp\{-bD_{slow}\}$ applied to the APGSTE data acquired for cyclohexane imbibed in RSO_3H-MM-SBA-15 catalysts with a) 150 nm macropores and b) 430 nm macropores, along with dodecane imbibed in RSO_3H-MM-SBA-15 catalysts with c) 150 nm macropores and d) 430 nm macropores. D_{fast} and D_{slow} values are given in **Table S2** and correspond to the limiting gradients at high and low b, respectively.

Table S2. Diffusion coefficients obtained from the biexponential fitting illustrated in **Figure S10**. Errors represent ± 1 standard deviation of 3 measurements obtained from 3 different samples.

Probe molecule	Macropore diameter / nm	Δ / ms	D_{fast} × 10^{10} / m^2 s^{-1}	D_{slow} × 10^{12} / m^2 s^{-1}	D_0/D_{fast}
Cyclohexane	150	25	2.59 ± 0.04	8.0 ± 0.3	4.98 ± 0.07
		50	2.56 ± 0.04	7.1 ± 0.3	5.05 ± 0.08
		100	2.54 ± 0.05	6.3 ± 0.3	5.07 ± 0.11
		200	2.55 ± 0.05	5.8 ± 0.3	5.06 ± 0.10
	430	25	3.91 ± 0.03	7.8 ± 0.3	3.30 ± 0.03
		50	3.90 ± 0.05	6.1 ± 0.3	3.31 ± 0.04
		100	4.00 ± 0.01	5.3 ± 0.3	3.23 ± 0.01
		200	4.07 ± 0.01	4.0 ± 0.3	3.17 ± 0.01
Dodecane	150	25	1.41 ± 0.03	7.3 ± 0.3	5.51 ± 0.10
		50	1.37 ± 0.02	6.3 ± 0.3	5.68 ± 0.09
		100	1.33 ± 0.02	5.9 ± 0.3	5.85 ± 0.10
		200	1.31 ± 0.02	5.0 ± 0.3	5.92 ± 0.11
	430	25	2.21 ± 0.02	6.8 ± 0.3	3.51 ± 0.03
		50	2.17 ± 0.02	5.6 ± 0.3	3.58 ± 0.01
		100	2.15 ± 0.01	4.6 ± 0.3	3.61 ± 0.01
		200	2.17 ± 0.01	2.9 ± 0.3	3.58 ± 0.01

Table S3. Spin-lattice relaxation time constants for restricted and unrestricted probe liquids as obtained using the inversion recovery sequence. Errors represent ± 1 standard deviation of 3 measurements performed on the same sample.

Probe Molecule	T_1 / s		
	Unrestricted liquid	Macropore diameter / nm	
		150	430
Cyclohexane	2.377 ± 0.003	1.97 ± 0.03	2.36 ± 0.04
Dodecane	1.345 ± 0.002	1.00 ± 0.02	1.15 ± 0.02

Table S4. Diffusion coefficients obtained from the 2-component anisotropic fitting illustrated in **Figure 5** in the main text. Note that $p_{iso} = 1 - p_{aniso}$. . Errors represent $\pm$ 1 standard deviation of 3 measurements obtained from 3 different samples. The root mean squared displacement is calculated as $RMSD = \sqrt[2]{2\Delta D}$. Values marked with a * are those given in Table 2 of the main text.

Probe molecule	Macropore diameter / nm	Δ / ms	p_{aniso}	D_{iso} × 10^{10} / m^2 s^{-1}	D_{par} × 10^{10} / m^2 s^{-1}	$RMSD_{iso}$ / μm	$RMSD_{par}$ / μm
Cyclohexane	150	25	0.15 ± 0.01	2.96 ± 0.01	7 ± 1	3.85 ± 0.02	6 ± 1
		50	0.14 ± 0.04	2.90 ± 0.04	6 ± 1	5.38 ± 0.08	8 ± 2
		100	0.12 ± 0.03	*2.86 ± 0.05	7 ± 1	7.56 ± 0.14	12 ± 2
		200	0.12 ± 0.02	2.83 ± 0.04	7.2 ± 0.7	10.65 ± 0.14	17 ± 4
	430	25	0.06 ± 0.01	*4.35 ± 0.02	6 ± 2	4.66 ± 0.02	6 ± 2
		50	0.04 ± 0.01	4.36 ± 0.06	6 ± 1	6.60 ± 0.09	8 ± 2
		100	0.04 ± 0.01	4.44 ± 0.03	6 ± 1	9.42 ± 0.06	11 ± 2
		200	0.04 ± 0.01	4.51 ± 0.03	6 ± 1	13.43 ± 0.09	15 ± 4
Dodecane	150	25	0.03 ± 0.01	1.46 ± 0.02	3.2 ± 0.7	2.70 ± 0.03	4 ± 1
		50	0.03 ± 0.01	1.41 ± 0.02	3 ± 1	3.75 ± 0.05	6 ± 2
		100	0.03 ± 0.01	*1.37 ± 0.02	3.6 ± 0.7	5.24 ± 0.07	8 ± 2
		200	0.03 ± 0.01	1.36 ± 0.02	3.1 ± 0.1	7.38 ± 0.09	11 ± 1
	430	25	0.02 ± 0.01	2.34 ± 0.02	4.5 ± 0.4	3.42 ± 0.02	5 ± 1
		50	0.02 ± 0.01	2.29 ± 0.01	6 ± 1	4.78 ± 0.03	8 ± 2
		100	0.01 ± 0.01	*2.27 ± 0.01	6.0 ± 0.6	6.73 ± 0.01	11 ± 1
		200	0.02 ± 0.01	2.28 ± 0.01	7 ± 3	9.55 ± 0.03	16 ± 7

Table S5. D_0/D_{iso} and D_0/D_{par} values obtained from the 2-component anisotropic fitting data given in **Table S4**. This data is plotted in **Figure 7** in the main text. Errors represent $\pm$ 1 standard deviation of 3 measurements obtained from 3 different samples. Values marked with a * are those given in Table 2 of the main text.

Probe molecule	Macropore diameter / nm	Δ / ms	D_0/D_{iso}	D_0/D_{par}
Cyclohexane	150	25	4.36 ± 0.02	1.9 ± 0.4
		50	4.45 ± 0.07	2.0 ± 0.4
		100	*4.51 ± 0.08	1.7 ± 0.2
		200	4.56 ± 0.06	1.8 ± 0.2
	430	25	*2.97 ± 0.01	2.0 ± 0.6
		50	2.96 ± 0.02	2.1 ± 0.6
		100	2.91 ± 0.02	2.2 ± 0.5
		200	2.86 ± 0.02	2.3 ± 0.6
Dodecane	150	25	5.32 ± 0.06	2.5 ± 0.6
		50	5.51 ± 0.07	2.3 ± 0.7
		100	*5.65 ± 0.08	2.2 ± 0.4
		200	5.70 ± 0.07	2.5 ± 0.1
	430	25	3.31 ± 0.02	1.7 ± 0.1
		50	3.39 ± 0.02	1.3 ± 0.3
		100	*3.42 ± 0.02	1.3 ± 0.1
		200	3.40 ± 0.01	1.2 ± 0.5